The feedback of solid friction on glacier sliding does not substantially modify the form of the friction law

J. P. Roldán-Blasco[1], F. Gimbert[1], O. Gagliardini[1], A. Gilbert[1]

[1]Univ. Grenoble Alpes, CNRS, IRD, IGE, 38000 Grenoble, France

Key Points:

- The feedback between solid friction and glacier flow is studied with an analytical and a numerical model
- The form of the friction law with solid friction is similar to the pure-sliding friction law
- We propose a new friction law which includes solid friction based on physical parameters

Corresponding author: J. P. Roldán-Blasco, `juan-pedro.roldan-blasco@univ-grenoble-alpes.fr`

Abstract

Current theories to describe friction of glaciers over hard beds are formulated on the basis that ice is free of debris and slides perfectly over the glacier bed. However, it is common to find basal layers of debris-laden ice or frozen patches that could exert additional resistance to glacier flow. We provide an analytical solution that accounts for the effect of solid friction in the framework of Weertman (1957). The presence of solid friction slows glacier sliding, however not as much as expected due to a decrease in basal ice viscosity. This arises because of the mechanical feedback that tangential stress has on the ice viscosity. We further study this problem under the added complexity of cavity formation using a numerical finite element model of glacier sliding over a sinusoidal bed under steady-state conditions. The law with solid friction retains the overall shape of the pure-sliding friction law, including the rate-weakening regime, and most of the changes can be explained via the modification of the scaling parameters of the friction law with the previously derived solutions. Finally, we provide parameterizations of glacier sliding with friction to be used in large scale flow models.

1 Introduction

The dynamics of temperate glaciers or glaciers with a temperate base is strongly influenced by the conditions close to the bed, e.g. type of bed, geometry, water pressure (Cuffey & Paterson, 2010). In this type of glaciers, internal deformation may only explain a small part of the surface velocity (Hooke et al., 1992; Doyle et al., 2018; Maier et al., 2019), and the rest of the surface velocity is attributed to sliding at the bed. At the large-scale of a few ice-thicknesses (hundreds to thousands of meters), sliding speed can be predicted using a friction law (e.g., Weertman, 1957; Lliboutry, 1968; Budd et al., 1979; Fowler, 1986a; Schoof, 2005; Gagliardini et al., 2007), which relates the sliding velocity to a surface friction acting on the bed, called basal drag. Such drag is generated by processes that occur around small scale bed irregularities (Weertman, 1957) at a meso-scale (of the order of few meter to tens of meters), where stress concentration reduces the viscosity of the ice and facilitates flow. The magnitude of stress concentration is given by the obstacles' shape and size, which are described with the distance between obstacles and the roughness defined as the obstacles aspect ratio. The rougher a bed, the higher the resistance to flow and the lower the basal velocity. In the above mentioned friction laws the glacier is assumed to be clean of debris and ice to bed friction is neglected, such that pure sliding is assumed at the ice-bed interface. As a result, bed shear stresses described by these theories are only produced by forces normal to the bed against the meso-scale obstacles.

There is evidence to consider the role of solid friction on glacier dynamics, originated by the contact between ice or sediments with the bedrock. In first place, debris carried by basal ice provide rock to rock friction. This has been observed for long in many mountain glaciers, see for instance the discussion in Alean et al. (1985), the images recorded at a natural cavity under Argentière Glacier in France (Figure 1), or the different studies carried out under the temperate glacier Engabreen (Norway), where records showed local tangential stress with a magnitude similar to the driving stress (Iverson et al., 2003; Cohen et al., 2005). In second place, indirect evidence is provided through seismic observations of basal stick-slip events emanating from the ice-bed interface suggesting that solid friction can act across large regions of the bed (Wiens et al., 2008; Zoet et al., 2012; Helmstetter et al., 2015; Roeoesli et al., 2016; Lipovsky et al., 2019). In third place, areas of the bed at sub-freezing temperatures can be local spots of high solid friction (Fowler, 1986b), since the friction between ice on rock is strongly dependant on the temperature of the ice, increasing rapidly with sub-freezing temperatures (McCarthy et al., 2017). Given that the choice of one glacier friction law over another has a significant impact on long term prognosis of the

Figure 1. Cavity under Argentière Glacier, french Alps. The debris cover visible at the base of the glacier varies in density during time. Photograph by Luc Moreau at `http://www.moreauluc.com/`

evolution of ice-sheets and glaciers and the computation of sea level rise (Ritz et al., 2015; Brondex et al., 2017, 2019; Nias et al., 2018; Joughin et al., 2019), it is important to determine whether solid friction significantly impacts the currently prescribed friction laws used in ice sheet models, so as to improve projections of glacier evolution and sea level rise.

Experimental investigations of the role of solid friction in glacier sliding have been mostly devoted to understand the micro-scale mechanisms that control solid friction (e.g. Cohen et al., 2005; Hansen & Zoet, 2019; Thompson et al., 2020). In comparison, several theoretical studies have tried to provide a meso-scale description, i.e. the friction law, for the case of ice flowing with solid friction. These have been done under the assumptions of ice as Newtonian fluid (Morland, 1976b; Hallet, 1979, 1981) or low concentration of debris in the absence of cavities (Fowler, 1986b) or with bed-separation (Iverson et al., 2019). As a consequence of assuming low concentrations of debris, the flow field can be assumed undisturbed and the same framework used to study the flow of ice over a frictionless interface can be used to study the case with solid friction. Solid friction can be integrated into the friction law just as a reduction in velocity and the same law as for the pure-sliding case can be applied, which seems to validate the aforementioned experimental observations.

In this paper, we study a friction law with and without cavities that includes solid friction, assuming non-linear ice and including for the first time the effect that the presence of solid friction has on the ice flow field (particularly the viscosity), explaining the changes this effect brings to the friction law. We start with a short background on friction laws and on the previous work which assesses solid friction. We then analytically and numerically derive friction laws that include solid friction. Finally, we discuss our findings in the context of ice dynamics and commonly described friction laws.

2 Rationale and Methodology

2.1 Glacier friction laws

The oldest friction law, and probably the most widely applied (see for instance Morlighem et al. (2013); Shapero et al. (2016); Larour et al. (2019)), has been proposed by Weertman (1957),

$$\tau_b = A_s^{-1/m} u_b^{1/m}, \tag{1}$$

where u_b is the basal velocity, τ_b the basal shear stress, m a material exponent, and A_s the sliding parameter which is dependant on the ice viscosity and bed geometry. Basal velocity and basal shear stress u_b and τ_b denote spatially averaged velocities and stresses in the flow direction close to the bed, respectively. If all basal drag is supported by the forces normal to the bed obstacles we have $m = n$, where n is the exponent of Glen flow law, the constitutive law commonly used for polycristaline ice. This exponent is typically considered equal to 3, but can vary between 2 - 4 (Cuffey & Paterson, 2010).

Many studies have been performed to improve Weertman's original expression for A_s for two-dimensional glaciers. Early mathematically sound works assumed ice as a linear (newtonian) fluid, (e.g. Kamb, 1970; Morland, 1976a), later extended to non-linear rheologies (Fowler, 1979). In general, in the hypothesis of very low roughness we have that A_s scales with $r^{-(n+1)}$ (Fowler, 1979), with r the bed roughness. Later studies, like Gudmundsson (1997a) or Gagliardini et al. (2007), have extended the analysis using numerical models that refine the expression of A_s.

This law does not take into account the role of water pressure p_w, which pushes against the ice pressure at the ice-bed interface, and reduces the contact pressure, called here effective pressure and denoted by N. If water pressure becomes higher than local ice pressure, the glacier separates from the bed and a cavity opens (Lliboutry, 1959; Lliboutry, 1968). This reduces the contact area and the apparent bed roughness, facilitating faster sliding (Lliboutry, 1968; Fowler, 1986a; Schoof, 2005; Gagliardini et al., 2007). In our analysis we compare our solution with the phenomenological law proposed by Gagliardini et al. (2007) for sliding over sinusoidal beds, given as

$$\frac{\tau_b}{\bar{N}} = C\left(\frac{\chi}{1+\alpha\chi^q}\right)^{1/n}, \text{ with } \chi = \frac{u_b}{C\bar{N}A_s}, \ \alpha = \frac{(q-1)^{q-1}}{q^q}. \tag{2}$$

Note that this law incorporates the spatially averaged effective pressure, $\bar{N}$. The bar marks the difference between local and meso-scale averaged effective pressures, N and $\bar{N}$. Parameter $C = max(\tau_b/\bar{N})$ is bounded by the maximum bed slope (Iken, 1981) and q is function of the slope severity index, which measures how steep the obstacles are for a given roughness (Gagliardini et al., 2007). In the case $q = 1$, $\tau_b/\bar{N}$ increases monotonically (Fowler, 1987; Schoof, 2005), while if $q > 1$ the law materializes two distinct behaviours. At low u_b the law follows equation (1), but as u_b increases due to the opening of cavities Weertman law under-represents the sliding velocity, see the shape of the law for different q in Figure 8 of Gagliardini et al. (2007). After the peak $\tau_b = \bar{N}C$ is reached, the law enters in the weakening range, as the bed cannot generate enough basal drag to balance driving stress for faster u_b, so τ_b has to be non-locally accommodated. This law is built to match the numerical results, and is based on the equation 6.2 proposed by Schoof (2005) which is, in the words of Schoof, "essentially the same as proposed by Fowler (1987)", a heuristic generalisation to non-linear ice of an equation that is able to reproduce fairly well the features of the semi-analytical solution for linear ice derived in Schoof (2005). This type of laws can be applied to three dimensional beds, as supported by laboratory experiments (Zoet & Iverson, 2015) and numerical simulations (Helanow et al., 2020), although the weakening range does not seem to hold for realistic beds with well-spaced non-periodic obstacles (Helanow et al., 2021).

2.2 Solid friction

A simple approach to incorporate solid friction on a glacier is to use a Coulomb friction law. This law provides the solid friction drag $\tau_f = \mu\bar{N}$ where μ is a homogeneous bulk friction parameter. The advantage of this description relies in its simplicity, since it only depends on one frictional parameter and on the effective pressure. If we assume that frictional drag is given by debris at the base, μ could range from $\mu = 0$ if there is no solid friction to $\mu \approx 0.6$ in the end member case of the glacier bottom being completely underlined by rocks.

Solid friction records of debris-laden ice on rock in natural settings (at Engabreen, Norway, Cohen et al. (2005)) report values about $\mu \approx 0.05$. Debris-free ice on rock can also have non negligible solid friction, even in temperate glaciers and under realistic sliding velocities, e.g. $\mu = 0.035$ for 15 ma^{-1} (McCarthy et al., 2017), although the literature is sometimes contradictory and recent experiments of temperate ice on rock show negligible friction values (Thompson et al., 2020). More complex models of friction between debris and the glacier bed are velocity dependant (e.g. Hallet, 1981; Cohen et al., 2005; Iverson et al., 2019), but for simplicity of deriving an analytical solution, we will consider a Coulomb friction law which can model solid friction regardless of how its generated. Since we expect the basal drag to depend on viscous drag (velocity dependant) and on solid friction (friction and effective pressure dependant), we can expect that the new friction law will be of the form $\tau_b/\bar{N} = f\left(u_b, \bar{N}, \mu\right)$. The next step is determining $f\left(u_b, \bar{N}, \mu\right)$.

2.3 Preliminary considerations

We consider a two-dimensional glacier of average thickness $H + h_i$ and surface slope θ contained in the $x - z$ plane and flowing over a periodic bed of height $z = b(x)$ and period L (see Figure 2 and Table 1 for the notation definition). Normal and tangential unit vectors at the domain boundary are denoted by $\mathbf{n}$ and $\mathbf{t}$, respectively. The bottom boundary of the ice is given by the periodic function $h(x) \geq b(x)$. We study a subdomain of the glacier, limited in width to L and in height to H, see Figure 2. Above H we assume that the flow field is undisturbed by the irregularities of the bed, such that at $z = H$ the stress and velocity fields are uniform. In this domain the Stokes flow equations are solved for the ice velocity $\mathbf{u}(x, z)$ and pressure $p(x, z)$ using Glen's law (Cuffey & Paterson, 2010) as constitutive law. The Cauchy stress tensor is denoted by $\boldsymbol{\sigma}$, normal stress at a surface is expressed as $\sigma_{nn} = \mathbf{n} \cdot \boldsymbol{\sigma}\mathbf{n}$ and shear stress as $\sigma_{nt} = \mathbf{t} \cdot \boldsymbol{\sigma}\mathbf{n}$. Periodic boundary conditions are applied on left and right sides, far field conditions are applied on the top boundary and correspond to overburden ice pressure $\sigma_{nn} = \bar{p_i} = -\rho_i g h_i cos(\theta)$ and uniform horizontal velocity u_i. The subglacial hydrological system is assumed perfectly spread along the bottom boundary at uniform pressure p_w. At the ice-bed interface the conditions are impenetrability, $\mathbf{u} \cdot \mathbf{n} = 0$ and shear stresses modeled with Coulomb friction law $\sigma_{nt} = -\mu(\sigma_{nn} - p_w)$. At the ice-cavity interface we impose that normal stress is equal to the cavity water pressure $\sigma_{nn} = -p_w$, and tangential stress is zero.

We can perform the balance of vertical and horizontal forces over the subdomain of study to gain some insights about the friction law with solid friction. We use the same procedure as that developed by Schoof (2005), considering the convention of negative stresses for compression, and normal and tangential vectors $\mathbf{n}$ and $\mathbf{t}$ with respect to the interface oriented as drawn in Figure 2.

Basal drag and overburden pressure are given by reaction forces at the bottom boundary

$$(-\tau_b, \bar{p_i}) = -\frac{1}{L}\int_{\delta\Omega_3} \sigma_{nn} + \sigma_{nt} ds. \tag{3}$$

Projecting into x and z, and separating between horizontal and vertical directions gives

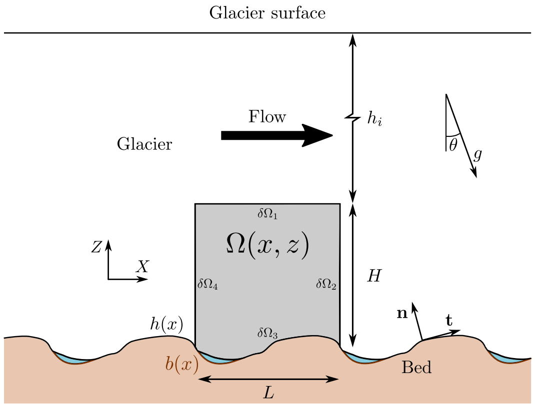

Figure 2. An example of a two-dimensional infinite glacier and the sub-domain of interest Ω (in gray). The example shows a vaguely sinusoidal bed in brown with water-filled cavities in blue.

$$\begin{cases} \tau_b = \dfrac{1}{L} \displaystyle\int_L h'(N + p_w) + \mu N \; dx \\ \bar{p_i} = \dfrac{1}{L} \displaystyle\int_L N + p_w - h'(\mu N) \; dx, \end{cases} \tag{4}$$

with $h'(x)$ the local slope of the bed. Notice that the integral of $h'p_w$ over the bed vanishes due to the periodicity of the bed. Using the expressions for the two different sources of drag averaged at the meso-scale, the viscous drag τ_u, caused by normal reactions σ_{nn} to the flow at the bed, and the solid friction drag τ_f, caused by local shear stresses σ_{nt} along the bed, which are

$$\tau_u = \frac{1}{L} \int_L h'N \; dx; \quad \tau_f = \mu \underbrace{\frac{1}{L} \int_L N \; dx}_{\bar{N}}, \tag{5}$$

we can rewrite equation (4) as

$$\begin{cases} \tau_b = \tau_u + \tau_f \\ \bar{p_i} - p_w = \bar{N} - \mu\tau_u \end{cases} \tag{6}$$

To further study the basal drag we introduce the reduced friction variable T,

$$T = \frac{\tau_f}{\tau_b}, 0 \leq T \leq 1. \tag{7}$$

Substituting equations (5) into τ_b in (6) allows us to identify the basal drag upper bound. Viscous drag is bounded by the slope and the effective pressure (Iken, 1981), so that for the first terms of the force balance we have $\tau_u < sup(h')\bar{N}$. The upper bound of the basal drag with solid friction $\tau_b \leq C_f \bar{N}$ can be found by just adding τ_f to both sides of the inequality, giving

$$C_f \leq sup(h'(x)) + \mu, \tag{8}$$

which is the expression suggested in Schoof (2005). If μ is distributed heterogeneously along the glacier bed we just replace μ by $max(\mu(x))$.

We can see that the presence of solid friction strengthens the bed, which now can support higher basal stress than a bed with a frictionless interface. We expect solid

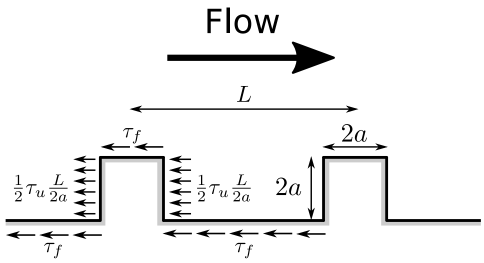

Figure 3. Continuous version of the tombstone model with the considered stresses.

friction to take up some of the drag that would otherwise be supported by normal reaction forces. For a given driving stress this would result in slower sliding speeds compared to the pure-sliding scenario, since now normal stress concentration is lower. In the following two sections we solve the flow of a glacier with solid friction and provide an analytical friction law for the case without cavities and a numerical friction law over sinusoidal beds which accounts for cavity opening.

3 Friction laws with solid friction

3.1 Analytical friction law in the absence of cavities

We study an idealized version of a glacier bed geometry that is similar to the 'tombstone model' considered in Weertman (1957) (see Figure 3 for a scheme of the bed with the stresses considered). The bed $b(x)$ is a rectangular function, of protuberances of side $2a$ separated between each other by a distance L, with roughness $r = a/L$. For this analytical solution we assume that i) the ice stays in contact with the bed everywhere (no open cavities), ii) viscous drag operates on the vertical sides of the bumps, and friction drag on the horizontal sides, and iii) the stress and strain fields are uniform over the domain of study. We use $u_b(T = 0)$ and A_s as notation for sliding speed and sliding parameter in a pure-sliding scenario. Likewise, $u_b(T)$ and A_f refer to the sliding speed and sliding parameter when there is solid friction.

Deviatoric stresses τ_{xx}, τ_{xz} and effective deviatoric stress τ_E are (Cuffey & Paterson, 2010)

$$\begin{aligned}
&\tau_{xx} = \frac{1}{2}\tau_u\frac{L}{2a},\ \tau_{zz} = -\tau_{xx},\ \tau_{yy} = 0,\\
&\tau_{xy} = 0,\ \tau_{xz} = \tau_f,\ \tau_{yz} = 0,\\
&\tau_E = (\frac{1}{16}\tau_u^2\frac{L^2}{a^2} + \tau_f^2)^{\frac{1}{2}}.
\end{aligned} \tag{9}$$

As formulated in section 2, the constitutive law for ice is given by Glen's law, such that

$$\dot{\varepsilon}_{ij} = A\tau_E^{n-1}\tau_{ij}, \tag{10}$$

where ice creep parameter A is considered as constant since the ice is assumed temperate. We see in equation (10) that ice deformation increases non-linearly with deviatoric stresses, meaning that a small increase in deviatoric stress induces a larger increment in strain rates. This will become relevant when we analyze the effect of solid friction on the sliding velocity.

Using equation (10) we obtain the following strain rates,

$$\dot{\varepsilon}_{xx} = A\left(\frac{1}{16}\tau_u^2\frac{L^2}{a^2} + \tau_f^2\right)^{\frac{n-1}{2}}\frac{1}{4}\tau_u\frac{L}{a}, \text{ and } \dot{\varepsilon}_{xz} = A\left(\frac{1}{16}\tau_u^2\frac{L^2}{a^2} + \tau_f^2\right)^{\frac{n-1}{2}}\tau_f, \tag{11}$$

corresponding to the pure-shear strain rates and the simple shear strain rates, respectively.

The sliding speed is evaluated as the integral of the strains along a distance L, at a thickness l within which most of the deformation caused by the presence of the bump is concentrated. This gives $u_b = \dot{\varepsilon}_{xx}L + 2\dot{\varepsilon}_{xz}l$.

As a first approximation, we consider that $l \propto L$ (Gudmundsson, 1997a). In particular, if we take $l = L/4$ (Lliboutry, 1968) and we rewrite to include the roughness $r = a/L$ we get

$$u_b = A\left(\frac{1}{16}\tau_u^2\frac{1}{r^2} + \tau_f^2\right)^{\frac{n-1}{2}}\frac{1}{4}\tau_u\frac{1}{r}L + A\left(\frac{1}{16}\tau_u^2\frac{1}{r^2} + \tau_f^2\right)^{\frac{n-1}{2}}\frac{1}{2}L\tau_f. \tag{12}$$

Substituting for the fraction of solid friction $T = \tau_f/\tau_b$ into equation (12) and factoring out common terms gives the sliding speed

$$u_b = A\left(\frac{1}{16}(1-T)^2\frac{1}{r^2} + T^2\right)^{\frac{n-1}{2}}\left(\frac{1}{4}(1-T)\frac{1}{r} + \frac{1}{2}T\right)L\tau_b^n. \tag{13}$$

For $T = 0$ we obtain, in agreement with Weertman (1957)

$$u_b(T=0) = \frac{1}{4^n}A\left(\frac{1}{r}\right)^n L\tau_b^n. \tag{14}$$

We can investigate the effect of solid friction on the flow speed. We do so through evaluating the ratio $(u_b(T)/\tau_b^n)/(u_b(T=0)/\tau_b^n) = A_f/A_s$, equivalent to the ratio $u_b(T)/u_b(T=0)$,

$$\frac{A_f}{A_s} = \underbrace{(1-T)^{\frac{2n}{n-1}}}_{\text{pure shear}} + \underbrace{16r^2(1-T)^{\frac{2}{n-1}}T^2 + 2r(1-T)^2T^{\frac{2}{n-1}}}_{\text{feedback terms}} + \underbrace{32r^3T^{\frac{2n}{n-1}}}_{\text{simple shear}}. \tag{15}$$

This is a decreasing function with T where the pure shear term is the leading term, while the rest partially mitigate the decrease in sliding speed that results from solid friction. If the roughness is very low this expression simplifies to $\lim_{r\to 0} A_f/A_s = (1-T)^{2n/(n-1)}$, as proposed by Fowler (1986b). In this case the decrease in sliding velocity is maximized and there is no compensation provided by the presence of tangential stress. The full expression is plotted for several values of n and for $r = 0.08$ in solid lines of the left panel of Figure 4, while the simplified expression $A_f/A_s = (1-T)^{2n/(n-1)}$ is in dotted lines. The difference between them is the combined effect of the simple shear deformation (almost negligible) and the feedback effect that solid friction has on basal sliding. We see in the left panel that for any n and except for $T \approx 1$, as solid friction increases so does the difference between the complete expression and the low roughness simplification. We show a particular case ($n = 3$ and $r = 0.08$) in the right hand panel to illustrate the individual contribution of each of the terms of equation (15) (notice that for any T, the cumulative sum of the terms is 100%). The pure-shear contribution, given by the black line, represents the change in velocity if we only consider the pure-shear (compression-extension) type of deformation. It decreases with increasing T, because more solid friction means less viscous drag and this is only possible if the sliding speed is lower. The two terms in the middle of equation (15) (represented by the dark green line) are called the feedback terms because they appear if we consider at

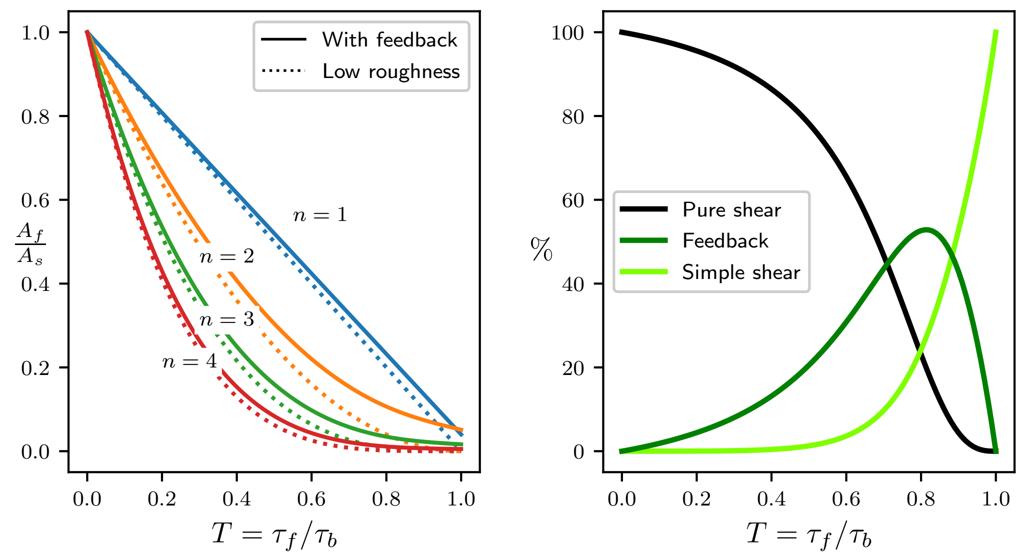

Figure 4. Left panel: Change in the sliding parameter for a Weertman tombstone model, for $r = 0.08$ and several values of n. The continuous lines 'with feedback' are the A_f/A_s curves including the feedback effect on viscosity given by τ_f, the last 3 terms of equation (15). The dotted line is for $A_f/A_s = (1-T)^{2n/(n-1)}$. Right panel: relative contribution to A_f/A_s of each term of equation (15), for $r = 0.08$ and $n = 3$.

the same time the effect of τ_u (normal stress) and τ_f (tangential stress) in ice viscosity. In particular, $16r^2(1-T)^{2/(n-1)}T^2$ shows how the pure-shear deformation is modified by the presence of tangential stress, and $2r(1-T)^2T^{2/(n-1)}$ shows how the simple-shear deformation is modified by normal stress. These terms are zero if $n = 1$, and for $n > 1$, and they are the second most important term of the reduction of sliding speed. The last term of A_f/A_s, represented by the light green line, is the contribution to the sliding velocity that comes from the simple shear type of deformation. It is very low since it grows with the third power of r, and therefore is the principal contributor to A_f/A_s only when $T \approx 1$ and the sliding velocity approaches zero. In this example we can see that if $T = 0.5$ (half the basal drag supported by solid friction), ignoring the feedback of solid friction introduces an error of about 20% in the sliding speed, with $(1-T)^3$ representing about 80% of the expected sliding speed.

We can rewrite equation (13) to obtain the final expression of the friction law with solid friction in the absence of cavities, expressed as

$$\tau_b = A_s^{\frac{-1}{n}} \left[(1-T)^{\frac{2n}{n-1}} + 16r^2(1-T)^{\frac{2}{n-1}}T^2 + 2r(1-T)^2T^{\frac{2}{n-1}} + 32r^3T^{\frac{2n}{n-1}} \right]^{\frac{n-1}{2n}} u_b^{\frac{1}{n}}. \quad (16)$$

For $n = 3$, a typical value in glacier models, the friction law with solid friction in the absence of cavities is

$$\tau_b = \left[A_s^{-1} \left((1-T)^3 + 16r^2(1-T)T^2 + 2r(1-T)^2T + 32r^3T^3 \right) u_b \right]^{\frac{1}{3}}. \quad (17)$$

3.2 Numerical friction law in the presence of cavities

To obtain the solution for the friction law including the effect of solid friction and the opening of cavities, we use the finite element method software Elmer/Ice (Gagliardini et al., 2013), with the same geometry but different boundary conditions to the sinusoidal bed studied in Gagliardini et al. (2007). The bed height function is a single wave function with amplitude a,

$$b(x) = asin\left(\frac{2\pi x}{L}\right). \tag{18}$$

We consider the same range of roughness as Gagliardini et al. (2007), between $r = 0.005$ and $r = 0.080$. The numerical domain is a regular mesh of bi-linear quadrilateral elements, vertically refined towards the bottom boundary. Most of the simulations The imposed boundary conditions at the top are horizontal velocity $u_i = 150$ ma^{-1} and ice pressure $p_i \approx 1.77$ MPa (the pressure caused by 200 meters of ice). At the bottom we explore different values of solid friction τ_f through varying the friction parameter, from $\mu = 0$ to $\mu = 0.15$ as well as by using 81 different values of p_w, with $\bar{N}$ ranging between $\bar{N} = 0.2p_i$ and $\bar{N} = p_i$, with increments every 1%. This combination of different roughness, friction parameter and effective pressure allows us to better constrain the friction law, since the changes introduced depend on r, μ and $\bar{N}$. For details on how u_b, τ_b and $\bar{N}$ are computed refer to Gagliardini et al. (2007) or Helanow et al. (2020). With prescribed $\bar{N}$ and μ, computing τ_f and therefore τ_u is straightforward, although in any case we can recover them from the stress tensor. The friction laws are shown in Figure 5. In all panels we add for comparison purposes the semi-analytical solution over a sinusoidal bed presented in Schoof (2005) (green line) and the phenomenological solution given by Equation (2) for $q = 1.8$ (blue line). Panel (a) evaluates friction laws through normalising by the pure-sliding friction parameters only, as done in Gagliardini et al. (2007). We observe that the shape of the law is conserved, but as we consider higher μ they are stretched in the vertical direction, showing that the maximum stress supported by the bed has increased due to the inclusion of τ_f. We can account for the change in maximum stress by combining equation (8) and the one proposed by Gagliardini et al. (2007) for C, which gives $C_f = \mu + k\pi r$, with k a constant. Performing a least squares regression on the $C_f = max(\tau_b/\bar{N})$ gives $k = 0.81$, which is not far from $k = 0.84 \pm 0.02$ as proposed in Gagliardini et al. (2007). We therefore conclude that for the maximum drag we have $C_f = C + \mu$ as expected from the theoretical considerations used to derive (8). In the following we use the maximum of each numerical simulation in order to ensure that all friction laws are capped at $\tau_b^3/(C_f\bar{N})^3$ as in Gagliardini et al. (2007).

To calculate the new sliding parameter A_f, we use the solution for the friction laws without cavities, equation (15), giving us the fitting function $A_f/A_s = (1-T)^3 + \beta r^2(1-T)T^2 + \gamma r(1-T)^2T$. The last term of the analytical solution is neglected to avoid over fitting, since it is expected to be very low except for $T \approx 1$. The factors that multiply the feedback terms are kept free in the fit, because their values will depend on the shape of the bed and on the strain field, much simplified in the analytical model. A quick check showed that the analytical expression (equation (15)) tended to underestimate the feedback in the numerical simulations. To obtain the data points A_f/A_s in the no-cavity regime, we compute $A_f(T)$ as the ratio between τ_b^n/u_b for those points of the tests with $\mu > 0$ that have a cavity extension lower than 1% of the bed wavelength. The pure sliding parameter A_s for each roughness is taken as the mean of the ratio τ_b^3/u_b for $p_w \in [0.03, 0.06]\, p_i$ for the $\mu = 0$ simulations. We avoid computing A_s with the solution for $p_w < 0.03p_i$ to avoid numerical artifacts observed in some of the pure-sliding tests with very low r. Some tests with roughness $r = 0.07$ and $r = 0.08$, and $\mu = 0.15$ had no basal sliding for high values of $\bar{N}$ and are not considered for the analysis. The results of the fit are $\beta = 65.9$ and $\gamma = 9.59$, which

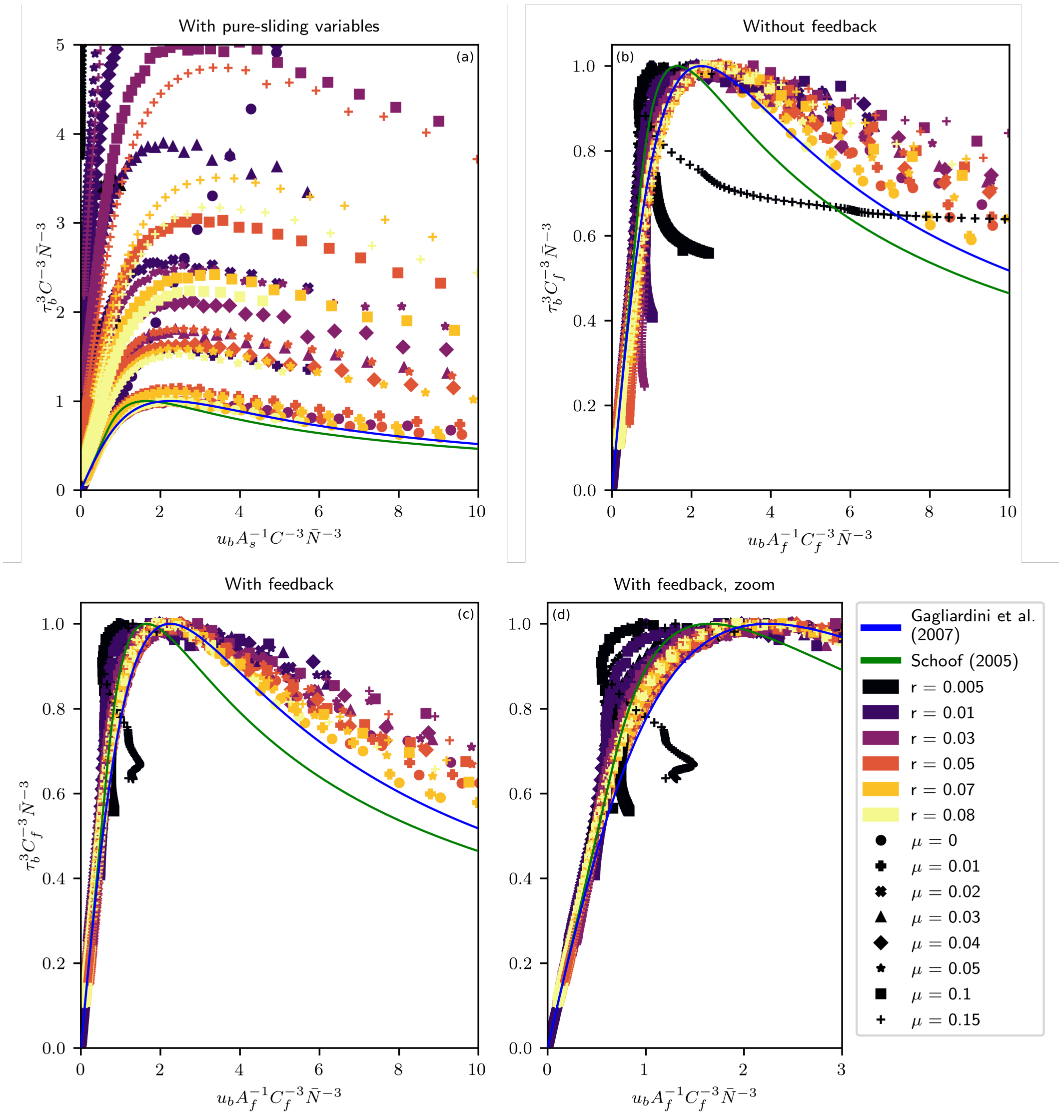

Figure 5. Numerical friction laws scaled using different criteria. Panel (a) shows the results if we use the same pure sliding parameters C and A_s as in the case $\mu = 0$. Panel (b) uses the stress bound C_f and A_f as if there was no feedback on viscosity ($\beta = \gamma = 0$) Panel (c) shows the friction law with the full corrected expression, in particular with $\beta = 65.9$ and $\gamma = 9.59$. Panel (d) shows a zoom into the rate-strengthening part of the friction law to show that we manage to generalize the friction law and approach all curves towards a shape similar to the the pure-sliding semi-analytical solution for a sinus bed of Schoof (2005, Figure 3 with $\alpha = \infty$) and the phenomenological law shown in equation (2) with $q = 1.8$ (Gagliardini et al., 2007). For panels (b) to (d), the scaling parameters for Gagliardini and Schoof curves are the same as in the pure-sliding case ($\mu = 0$), as that is the process they describe.

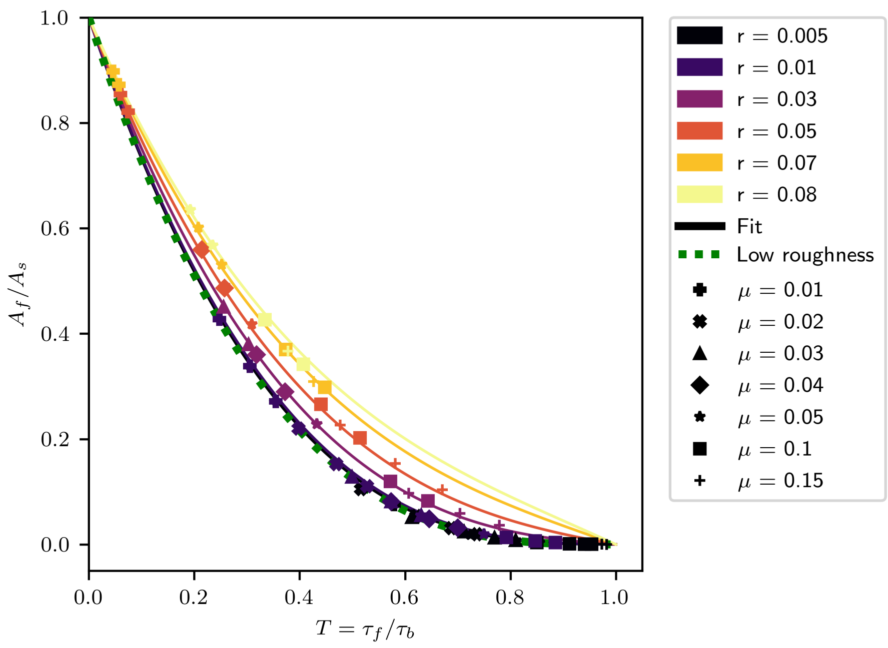

Figure 6. Numerical A_f/A_s and the fit obtained after performing a least-squares regression on the numerical data, using a modification of the analytical solution. For every test with the same r and μ we only show one of every 20 data points for clarity. The blue continuous curve, corresponds to the low roughness approximation ($A_f/A_s = (1-T)^3$).

is approximately four times greater than the corresponding values obtained with the tombstone analytical solution. The fit can be seen in Figure 6 alongside with some of the data used to obtain it. Once both C_f and A_f for the numerical tests are found, we proceed to compare the friction laws with and without the solid friction feedback. In panel (b) of Figure 5 we see the laws normalised by $C_f = max(\tau_b/\bar{N})$ and $A_f = A_s(1-T)^3$, and in panel (c) and the zoom in (d) the laws normalised by $C_f = max(\tau_b/\bar{N})$ and $A_f = A_s\left[(1-T)^3 + 65.9r^2(1-T)T^2 + 9.59r(1-T)^2T\right]$.

We show the friction laws with different scalings alongside the semi-analytical solution for linear ice given in Schoof (2005), and equation (2) for $q = 1.8$. The numerical friction laws with solid friction, once properly scaled, show a good collapse onto the same general shape, similar to the semi-analytical solution for linear ice of Schoof (2005) and the formulation proposed by Gagliardini et al. (2007) with $q = 1.8$. The basal velocity in the weakening regime is consistently underestimated in both friction laws. The feedback terms improve the collapse (compare the rate-strengthening part of the friction laws in panels (b) and (c) of Figure 5). Ignoring the feedback of solid friction in the viscosity introduces some error in the shape of the friction laws, and the expected velocity is lower than the observed velocity. The sliding parameter associated with the lowest roughness $r = 0.005$ is very sensitive to small absolute errors in A_f, therefore we are not able to describe it as successfully as for the other roughness.

We propose the following update to the phenomenological friction law proposed in Gagliardini et al. (2007) for sinusoidal beds and $n = 3$, with the two new scaling variables C_f and A_f that take into account solid friction,

$$
\begin{aligned}
\tau_b &= C_f \bar{N} \left(\frac{\chi}{1+\alpha\chi^2} \right)^{1/3}, \chi = \frac{u_b}{C_f \bar{N} A_f}, C_f = C_s + \mu, \\
A_f &= A_s \left[(1-T) + 65.9 r^2 (1-T) T^2 + 9.59 r (1-T)^2 T \right], T = \frac{\mu \bar{N}}{\tau_b}
\end{aligned}
\tag{19}
$$

4 Discussion

We demonstrate the friction law including solid friction can be generalized for any roughness r, basal slip u_b, and solid friction drag τ_f that is considered. The new element introduced in the friction law is the feedback on viscosity, ignored in previous models that assumed low concentration of debris. The main effect of having solid friction is that the glacier slows down, but this decrease in velocity is partially compensated by the stress tensor becoming more deviatoric as a result of the additional shear stress, so that including solid friction without its feedback on viscosity will underestimate the sliding velocity. The analytical study shows the law can be updated by simply changing the scaling parameters C and A_s formulated in previous studies that neglected solid friction into C_f and A_f which are now functions of the bed roughness r and a variable T, which corresponds to the ratio between solid friction drag and basal drag. The numerical simulations show that the analytical correction of the sliding parameter found here for the case without cavities is applicable to sliding with cavities. The corrected friction law behaves similarly to the pure-sliding case, such that the weakening regime is not suppressed by adding solid friction, building upon the conclusions drawn by Iverson et al. (2019) in a model that ignored the feedback. Given that the analytical model is formulated for different values of the flow exponent n, we expect that our conclusions drawn from the numerical simulations with $n = 3$ can be extended to other values of n, as it was already shown for the pure-sliding case in Gagliardini et al. (2007), so that the update to the friction law with solid friction proposed in equation (19) can be used as a reference.

The feedback effect in the numerical simulations is stronger than in the analytical model, as evidenced by the feedback factors β and γ in equation (15), which are approximately four times higher than in the tombstone model. This means that the analytical model overestimates the sliding velocity for a sinusoidal bed, specially in the pure-sliding case, but the form of the law is the same and the same method could be applied to derive A_f for other types of bed, i.e. more realistic 3-D bed for example. We expect that this discrepancy between the analytical and the numerical model lies in the assumption that the stress and strain-rates fields are uniform along a height $L/4$, as well as in the simplified treatment of the geometry. The stress was assumed uniform along a thickness $l = L/4$ and equal to the stress at the bed, when in reality we expect it to become closer to a simple-shear stress state as we move far from the ice-bed interface, so that the actual effective deviatoric stress and the strain rates are lower than assumed. This also highlights the difference between our analytical model where the basal slip is taken at a certain distance from the bed, and the numerical model where it is computed at the actual ice-bed interface as done in Gudmundsson (1997b); Gagliardini et al. (2007); Helanow et al. (2020, 2021), which provides a lower value for u_b than if done at a higher distance from the bed. The influence of the geometry (tombstone vs sinusoidal) can be partially understood with the same argument as the one used by Lliboutry (1968) to find two different estimates for the basal drag generated at a sinusoidal bed for a fixed basal speed. The first assumes a bed of constant slope (essentially our solution), while the other is an end-member that takes into account the zone of maximum stresses in a sinusoidal bed. The ratio between the estimated drags is 1.35, which means that at equal basal drag, the speed computed with our model can be up to $1.35^3 = 2.46$ times higher than in a model that accounts for the slope variability. The detailed solution of Lliboutry (1968) differs from ours in some details (he assumed plane strain rather than plane stress, for instance), but it shows that an analytical solution like the one we used has the tendency to overestimate the sliding velocity. We note as well that our simulations converge on a solution indicating that a force balance under steady condition is reached, so that the difference between solutions cannot be due to numerical artefacts.

We have seen that the forms of a pure-sliding friction law and a friction law with solid friction are very similar, complicating the identification of the presence or not of solid friction. A way to determine the contribution of solid friction based on field observations would be to identify the change in the sliding parameter, although such a task would likely be challenging given that it would require i) our model to reproduce with good accuracy the dynamics of a real glacier and ii) the data (velocities, basal drag and water pressure) to be representative enough of the glacier dynamics for the changes in the slope of the friction law to be attributed to the presence of solid friction and the associated change in viscosity.

The fundamental difference between a friction law with a velocity dependant model or an effective pressure dependant model of solid friction should be in how T evolves with the friction law. In our pressure dependant model, we observe that solid friction decreases with increasing velocity and/or water pressure while there are no cavities and then stabilizes as cavities open. Interestingly, a velocity dependant model of solid friction such as the one studied in Iverson et al. (2019), and considered in Thompson et al. (2020), is not very sensitive to basal slip, because as cavities grow, the increase in drag with increasing velocity balances out with the decrease in contact area. A simple solution could be to impose a constant solid friction τ_f, such that T stays constant until the peak is reached. This would simplify the influence that the viscosity feedback has on the shape of the friction law, since A_f would be constant, and the new friction law would be equal to a pure-sliding law. We remark that the numerical model already considers a heterogeneous distribution of tangential stresses, which is advantageous over uniform descriptions of solid friction (Hallet, 1979, 1981; Cohen et al., 2005; Iverson et al., 2019).

Our friction law has been formulated under steady-state conditions and may differ drastically under non-steady conditions, since the two sources of basal drag presently consider behave at very different timescales. On one hand, viscous drag is linked to the basal velocity, and therefore to the inertia of the ice, so that it will need some time to adapt to fast changes in water pressure or bed shear stress. On the other hand, we can expect that solid friction drag reacts instantaneously due to its dependence on the contact force between ice and bed. This difference in time scales can therefore be key when studying the behaviour of a glacier under unsteady conditions, while the glacier transitions from one steady state to another. Similarly, we don't expect that the presently established law applies to the case of highly concentrated debris at the glacier base that would make the material behave differently than a viscous fluid.

With regards to the bed geometry we await that our results are valid for other geometries, both 2-D and 3-D. For 3-D beds, the slope severity is restricted to a smaller area of the bed (Helanow et al., 2020) and therefore forces are more concentrated. As such, for the same basal drag, local normal stresses (and tangential if solid friction is assumed) are higher than for 2-D beds. This would make the stress state more deviatoric, and the viscosity feedback more important. Studying this type of settings where the basal drag is concentrated in small areas of the bed could also help understanding local tangential stresses higher than average drag, as was observed in Cohen et al. (2005). This possible stronger feedback in a more realistic 3-D bed could be balanced out by an ice with higher Glen flow law exponent n, as evidenced in some parts of Greenland (Gillet-Chaulet et al., 2011). A fast assessment of this is given in the left panel of Figure 4, where we showed that as n increases, the feedback effect tends to dissipate.

5 Conclusions

In this study, we developed a new analytical model of glacier sliding with solid friction that includes the effects on viscosity. We demonstrate that the analytical model can be used as basis to describe sliding with solid friction and cavities, as shown by our numerical simulations over sinusoidal beds. The analytical model shows that the pure-sliding derived friction laws can be easily adapted to accurately describe sliding with solid friction in the absence of cavities, while the numerical models shows that our proposed friction law can be extended to model the flow with cavities. Our findings on the form of the friction law are coherent to the models proposed in the literature that assumed low quantities of solid friction. Under this assumption, ice creep dominates sliding and solid friction can be understood as a reduction in basal drag. We extend these results by showing that if solid friction represents a significant portion of the total basal drag, the sliding velocity will not be as low as expected due to a mechanical feedback that reduces the ice viscosity. Ice creep around obstacles and cavities will still be representative of the sliding process even under high amounts of solid friction. As a result, the friction law with solid friction over a sinusoidal bed retains the overall shape when compared to the pure-sliding case, including the weakening behaviour. Further work has to be carried out to confirm up to what extent the results can be generalised to more realistic models of solid friction, how the interplay between solid friction and water pressure modifies the flow dynamics, and how important the feedback can be when sliding over realistic 3-D beds.

Acknowledgments

This work was supported by the French National Research Agency project SAUSSURE (ANR-18-CE01-0015-01). The authors would like to thank Nathan Maier and Christian Vincent for their useful comments and help. JPRB was in charge of developing the analytical model and doing the simulations. FG and OG designed the project, and OG helped with setting up the numerical simulations. All authors contributed to the analysis of the results and the writing of the paper. The numerical output and the scripts used to generate and process will be accessible upon publication in the long-term open access data repository "Zenodo community of the French ANR project SAUSSURE".

References

Alean, P., Braun, S., Iken, A., Schram, K., & Zwosta, G. (1985). Hydraulic Effects at the Glacier Bed and Related Phenomena. , *90*(90).

Brondex, J., Gagliardini, O., Gillet-Chaulet, F., & Durand, G. (2017, oct). Sensitivity of grounding line dynamics to the choice of the friction law. *Journal of Glaciology*, *63*(241), 854–866. doi: 10.1017/jog.2017.51

Brondex, J., Gillet-Chaulet, F., & Gagliardini, O. (2019, jan). Sensitivity of centennial mass loss projections of the Amundsen basin to the friction law. *Cryosphere*, *13*(1), 177–195. doi: 10.5194/tc-13-177-2019

Budd, W. F., Keage, P. L., & Blundy, N. A. (1979, jan). Empirical Studies of Ice Sliding. *Journal of Glaciology*, *23*(89), 157–170. doi: 10.3189/S0022143000029804

Cohen, D., Iverson, N. R., Hooyer, T. S., Fischer, U. H., Jackson, M., & Moore, P. L. (2005). Debris-bed friction of hard-bedded glaciers. *Journal of Geophysical Research: Earth Surface*, *110*(2). doi: 10.1029/2004JF000228

Cuffey, K., & Paterson, W. (2010). *Physics of Glaciers I* (No. I).

Doyle, S. H., Hubbard, B., Christoffersen, P., Young, T. J., Hofstede, C., Bougamont, M., ... Hubbard, A. (2018). Physical Conditions of Fast Glacier Flow: 1. Measurements From Boreholes Drilled to the Bed of Store Glacier, West Greenland. *Journal of Geophysical Research: Earth Surface*, *123*(2), 324–348.

Variable	Description	Unit
A	Rate factor	$\mathrm{MPa^{-n}a^{-1}}$
A_s	Sliding parameter in the pure-sliding case	$\mathrm{ma^{-1}\ MPa^{-n}}$
A_f	Sliding parameter if sliding with friction	$\mathrm{ma^{-1}\ MPa^{-n}}$
a	Half bump height, sinus amplitude	m
$b(x)$	Bed height	m
C	Maximum attainable $\tau_u/\bar{N}$	-
C_f	Maximum attainable $\tau_b/\bar{N}$	-
H	Top boundary height	m
h_i	Height of the ice column	m
$h(x)$	Cavity roof height	m
$h'(x)$	Slope of the ice-bed interface, dh/dx	-
L	Domain period length, bed wavelength	m
$\boldsymbol{n}$	Normal vector	-
n	Glen flow law exponent	-
N	Effective pressure	MPa
$\bar{N}$	Mean effective pressure	MPa
p	Flow pressure	MPa
p_i	Ice column pressure	MPa
p_w	Subglacial water pressure	MPa
r	Bed roughness, a/L	-
T	Reduced friction, τ_f/τ_b	-
$\boldsymbol{t}$	Tangential vector	-
$\mathbf{u}$	Flow velocity vector	$\mathrm{ma^{-1}}$
u	Horizontal component of $\mathbf{u}$	$\mathrm{ma^{-1}}$
u_i	Ice velocity at top boundary	$\mathrm{ma^{-1}}$
u_b	Basal slip	$\mathrm{ma^{-1}}$
$\bar{u}$	Far field velocity	$\mathrm{ma^{-1}}$
v	Vertical component of $\mathbf{u}$	$\mathrm{ma^{-1}}$
β	Viscosity modifier 1	-
γ	Viscosity modifier 2	-
μ	Bulk friction parameter	-
τ_b	Basal drag	MPa
τ_u	Viscous drag	MPa
τ_f	Solid friction drag	MPa
$\boldsymbol{\sigma}$	Cauchy stress tensor	MPa

Table 1. Table of variables

doi: 10.1002/2017JF004529

Fowler, A. C. (1979). A Theoretical Treatment of the Sliding of Glaciers in the Absence of Cavitation. , *298*(1445), 32,117. doi: 10.1098/rspa.1986.0090

Fowler, A. C. (1986a). A sliding law for glaciers of constant viscosity in the presence of subglacial cavitation. *Proceedings - Royal Society of London, Series A*, *407*(1832), 147–170. doi: 10.1098/rspa.1986.0090

Fowler, A. C. (1986b, jan). Sub-Temperate Basal Sliding. *Journal of Glaciology*, *32*(110), 3–5. doi: 10.3189/S0022143000006808

Fowler, A. C. (1987). Sliding with Cavity Formation. *Journal of Glaciology*, *33*(115), 255–267. doi: 10.3189/s0022143000008820

Gagliardini, O., Cohen, D., Råback, P., & Zwinger, T. (2007, jun). Finite-element modeling of subglacial cavities and related friction law. *Journal of Geophysical Research: Earth Surface*, *112*(2). doi: 10.1029/2006JF000576

Gagliardini, O., Zwinger, T., Gillet-Chaulet, F., Durand, G., Favier, L., de Fleurian, B., … Thies, J. (2013, aug). Capabilities and performance of Elmer/Ice, a new-generation ice sheet model. *Geoscientific Model Development*, *6*(4), 1299–1318. doi: 10.5194/gmd-6-1299-2013

Gillet-Chaulet, F., Hindmarsh, R. C. A., Corr, H. F. J., King, E. C., & Jenkins, A. (2011). In-situ quantification of ice rheology and direct measurement of the Raymond Effect at Summit, Greenland using a phase-sensitive radar. *Geophysical Research Letters*, *38*(24). doi: https://doi.org/10.1029/2011GL049843

Gudmundsson, G. H. (1997a). Basal-flow characteristics of a linear medium sliding frictionless over small bedrock undulations. *Journal of Glaciology*, *43*(143), 71–79. doi: 10.1017/s0022143000002823

Gudmundsson, G. H. (1997b). Basal-flow characteristics of a non-linear flow sliding frictionless over strongly undulating bedrock. *Journal of Glaciology*, *43*(143), 80–89. doi: 10.1017/s0022143000002835

Hallet, B. (1979, jan). A Theoretical Model of Glacial Abrasion. *Journal of Glaciology*, *23*(89), 39–50. doi: 10.3189/S0022143000029725

Hallet, B. (1981). Glacial Abrasion and Sliding: their Dependence on the Debris Concentration in Basal Ice. *Annals of Glaciology*. doi: 10.3189/172756481794352487

Hansen, D. D., & Zoet, L. K. (2019). Experimental constraints on subglacial rock friction. *Annals of Glaciology*, *60*(80), 37–48. doi: 10.1017/aog.2019.47

Helanow, C., Iverson, N. R., Woodard, J. B., & Zoet, L. K. (2021). Slip laws for bed-bedded glaciers derived from actual bed topography. *Science Advances*(May), 2–10.

Helanow, C., Iverson, N. R., Zoet, L. K., & Gagliardini, O. (2020). Sliding Relations for Glacier Slip With Cavities Over Three-Dimensional Beds. *Geophysical Research Letters*, *47*(3). doi: 10.1029/2019GL084924

Helmstetter, A., Nicolas, B., Comon, P., & Gay, M. (2015). Basal icequakes recorded beneath an alpine glacier (Glacier d'Argentière, Mont Blanc, France): Evidence for stick-slip motion? *Journal of Geophysical Research: Earth Surface*, *120*(3), 379–401. doi: 10.1002/2014JF003288

Hooke, R. L., Pohjola, V. A., Jansson, P., & Kohler, J. (1992). Intra-seasonal changes in deformation profiles revealed by borehole studies, Storglaciaren, Sweden. *Journal of Glaciology*, *38*(130), 348–358. doi: 10.1017/S0022143000002239

Iken, A. (1981, jan). The Effect of the Subglacial Water Pressure on the Sliding Velocity of a Glacier in an Idealized Numerical Model. *Journal of Glaciology*, *27*(97), 407–421. doi: 10.3189/S0022143000011448

Iverson, N. R., Cohen, D., Hooyer, T. S., Fischer, U. H., Jackson, H., Moore, P. L., … Kohler, J. (2003). Effects of basal debris on glacier flow. *Science*, *301*(5629), 81–84. doi: 10.1126/science.1083086

Iverson, N. R., Helanow, C., & Zoet, L. K. (2019). Debris-bed friction during glacier sliding with ice-bed separation. *Annals of Glaciology*, *60*(80), 30–36. doi: 10.1017/aog.2019.46

Joughin, I., Smith, B. E., & Schoof, C. G. (2019). Regularized Coulomb Friction Laws for Ice Sheet Sliding: Application to Pine Island Glacier, Antarctica. *Geophysical Research Letters*, *46*(9), 4764–4771. doi: 10.1029/2019GL082526

Kamb, B. (1970). Sliding motion of glaciers: Theory and observation. *Reviews of Geophysics*, *8*(4), 673–728. doi: 10.1029/RG008i004p00673

Larour, E., Seroussi, H., Adhikari, S., Ivins, E., Caron, L., Morlighem, M., & Schlegel, N. (2019). Slowdown in Antarctic mass loss from solid Earth and sea-level feedbacks. *Science*, *364*(6444). doi: 10.1126/science.aav7908

Lipovsky, B. P., Meyer, C. R., Zoet, L. K., McCarthy, C., Hansen, D. D., Rempel, A. W., & Gimbert, F. (2019). Glacier sliding, seismicity and sediment entrainment. *Annals of Glaciology*, *60*(79), 182–192. doi: 10.1017/aog.2019.24

Lliboutry, L. (1959, January). Une théorie du frottement du glacier sur son lit. *Annales de Geophysique*, *15*, 250.

Lliboutry, L. (1968). General Theory of Subglacial Cavitation and Sliding of Temperate Glaciers. *Journal of Glaciology*. doi: 10.3189/s0022143000020396

Maier, N., Humphrey, N., Harper, J., & Meierbachtol, T. (2019, jul). Sliding dominates slow-flowing margin regions, Greenland Ice Sheet. *Science Advances*, *5*(7), eaaw5406. doi: 10.1126/sciadv.aaw5406

McCarthy, C., Savage, H., & Nettles, M. (2017). Temperature dependence of ice-on-rock friction at realistic glacier conditions. *Philosophical Transactions of the Royal Society A: Mathematical, Physical and Engineering Sciences*, *375*(2086). doi: 10.1098/rsta.2015.0348

Morland, L. W. (1976a, jan). Glacier Sliding Down an Inclined Wavy Bed. *Journal of Glaciology*, *17*(77), 447–462. doi: 10.1017/S0022143000013733

Morland, L. W. (1976b, jan). Glacier Sliding Down an Inclined Wavy Bed With Friction. *Journal of Glaciology*, *17*(77), 463–477. doi: 10.3189/S0022143000013745

Morlighem, M., Seroussi, H., Larour, E., & Rignot, E. (2013). Inversion of basal friction in Antarctica using exact and incomplete adjoints of a higher-order model. *Journal of Geophysical Research: Earth Surface*, *118*(3), 1746–1753. doi: 10.1002/jgrf.20125

Nias, I. J., Cornford, S. L., & Payne, A. J. (2018). New Mass-Conserving Bedrock Topography for Pine Island Glacier Impacts Simulated Decadal Rates of Mass Loss. *Geophysical Research Letters*, *45*(7), 3173–3181. doi: 10.1002/2017GL076493

Ritz, C., Edwards, T. L., Durand, G., Payne, A. J., Peyaud, V., & Hindmarsh, R. C. (2015). Potential sea-level rise from Antarctic ice-sheet instability constrained by observations. *Nature*. doi: 10.1038/nature16147

Roeoesli, C., Helmstetter, A., Walter, F., & Kissling, E. (2016). Meltwater influences on deep stick-slip icequakes near the base of the Greenland Ice Sheet. *Journal of Geophysical Research: Earth Surface*, *121*(2), 223–240. doi: 10.1002/2015JF003601

Schoof, C. (2005, mar). The effect of cavitation on glacier sliding. *Proceedings of the Royal Society A: Mathematical, Physical and Engineering Sciences*, *461*(2055), 609–627. doi: 10.1098/rspa.2004.1350

Shapero, D. R., Joughin, I. R., Poinar, K., Morlighem, M., & Gillet-Chaulet, F. (2016). Basal resistance for three of the largest Greenland outlet glaciers. *Journal of Geophysical Research F: Earth Surface*. doi: 10.1002/2015JF003643

Thompson, A. C., Iverson, N. R., & Zoet, L. K. (2020). Controls on Subglacial Rock Friction: Experiments With Debris in Temperate Ice. *Journal of Geophysical Research: Earth Surface*, *125*(10), 1–18. doi: 10.1029/2020JF005718

Weertman, J. (1957). On the Sliding of Glaciers. *Journal of Glaciology*. doi: 10

.3189/s0022143000024709
Wiens, D. A., Anandakrishnan, S., Winberry, J. P., & King, M. A. (2008). Simultaneous teleseismic and geodetic observations of the stick-slip motion of an Antarctic ice stream. *Nature*, *453*(7196), 770–774. doi: 10.1038/nature06990
Zoet, L. K., Anandakrishnan, S., Alley, R. B., Nyblade, A. A., & Wiens, D. A. (2012). Motion of an Antarctic glacier by repeated tidally modulated earthquakes. *Nature Geoscience*, *5*(9), 623–626. doi: 10.1038/ngeo1555
Zoet, L. K., & Iverson, N. R. (2015, jul). Experimental determination of a double-valued drag relationship for glacier sliding. *Journal of Glaciology*, *61*(225), 1–7. doi: 10.3189/2015JoG14J174